



Giant vertical magnetization shift induced by spin canting in a Co/Ca₂Ru_{0.98}Fe_{0.02}FeO₄ heterostructure

S. J. Yuan,^{1,2,*} L. Li,² T. F. Qi,² L. E. DeLong,² and G. Cao²

¹Department of Physics, Shanghai University, Shanghai 200444, China

²Department of Physics and Astronomy and Center for Advanced Materials, University of Kentucky, Lexington, Kentucky 40506, USA

(Received 4 June 2013; published 15 July 2013)

We present a study of exchange bias generated at the interface between a polycrystalline Co film sputtered on a cleavage plane of single-crystal Ca₂Ru_{0.98}Fe_{0.02}FeO₄. The exchange bias is accompanied by an extremely large vertical magnetization shift that is characterized by 60% of the saturation magnetization in a 70-kOe cooling field. This phenomenon is seldom observed in other heterostructures. The effects of cooling-field amplitude and temperature on the exchange bias indicate that the magnetization shift results from a ferromagnetic contribution of canted moments in Ca₂Ru_{0.98}Fe_{0.02}O₄. A Type-I training effect is also observed, in which the hysteresis loop shrinks from both sides with cycling of the applied field.

DOI: [10.1103/PhysRevB.88.024413](https://doi.org/10.1103/PhysRevB.88.024413)

PACS number(s): 75.70.Cn, 75.30.Et, 75.60.Ej, 71.70.Ej

I. INTRODUCTION

Exchange bias (EB) refers to an overall shift of the magnetic hysteresis loop along the magnetic field axis in a system with an interface between ferromagnetic (FM) and antiferromagnetic (AFM) materials.¹ It is energetically favorable for a FM film to be magnetized in the direction of the external magnetic field \mathbf{H} in which it was cooled; and EB makes it appear as if an additional magnetic field were present in addition to the externally applied magnetic field at $T \ll T_N$, the Néel temperature of the antiferromagnet. Microscopically, EB is a result of spin-pinning effects at the FM/AFM interface, which results in a unidirectional exchange anisotropy H_E that competes with the applied magnetic field.^{2,3} Specifically, uncompensated AFM spins at the interface generate a net magnetic moment that is expected to pin the nearest-neighbor FM spins via an interfacial exchange coupling, giving rise to a preferred direction for the FM moments. This phenomenological model qualitatively captures the essential physics of EB, but grossly exaggerates the EB effect by several orders of magnitude compared to experimental results,²⁻⁴ and, more importantly, it fails to account for a *vertical magnetization shift* (VMS), which is the central issue addressed in this study.

A VMS has been observed frequently,⁵⁻¹⁶ and could originate from any of several proposed mechanisms. Among them, the Meiklejohn-Bean model predicts that an AFM monolayer at the interface with the FM layer is uncompensated, but still remains part of the AFM lattice.^{1,3} One could expect a contribution to the macroscopic or microscopic magnetization equal to that of the net magnetization of the uncompensated AFM monolayer so long as the AFM lattice consists of an odd number of monolayers. In the case of the Mauri mechanism,¹⁷ the AFM interface is compensated, and is unlikely to result in a VMS of the hysteresis loop. Nevertheless, a small VMS could be intrinsic to a multidomain state,^{6,7} spin glass,^{11,13,14} and the Malozemoff¹⁸ models for EB. At the interface between the AFM and FM layer, a number of frozen AFM spins will be uncompensated due to a proximity coupling with the FM layer, and they will contribute to the magnetization of the overall system: In the case of FM coupling, the overall hysteresis loop should be shifted upwards along the magnetization axis, whereas in the case of AFM coupling, the magnetization

curve should be shifted downwards.⁵ Nevertheless, because of uncompensated or compensated AFM and not-well-ordered interfacial spins, it is challenging to propose a comprehensive model to explain all the VMS behaviors.

Unfortunately, the VMS in conventional FM/AFM film heterostructures is considerably small and cannot be easily probed by isothermal magnetization measurements. Here we report a giant VMS in Co/Ca₂Ru_{0.98}Fe_{0.02}O₄ heterostructure. Ca₂Ru_{1-x}Fe_xO₄ was reported to be a spin-canted, G-type AFM.¹⁹ The effect of a net magnetization generated by spin canting on EB has not been studied, and a novel type of EB might be expected in such a system. We therefore deposited a FM Co film directly on the surface of single-crystal Ca₂Ru_{1-x}Fe_xO₄ to form an AFM/FM interface. We have indeed observed an EB with a strikingly large VMS of up to 60% of the net saturation magnetization, which we attribute to the unique spin-canted AFM structure of Ca₂Ru_{1-x}Fe_xO₄.

II. EXPERIMENTAL DETAILS

Single crystals of Ca₂Ru_{0.98}Fe_{0.02}O₄ were grown using a floating-zone optical furnace; details of single-crystal growth are described elsewhere.¹⁹⁻²¹ Chemical compositions were determined by energy dispersive x-ray (EDX) analysis, and structures by single-crystal x-ray diffraction; results of both measurements confirmed the high homogeneity of the single crystals. The single crystals were cleaved for use as substrates, and then precleaned by RF resputtering at 25 W for 5 min prior to Co film deposition by magnetron sputtering. Because of the negative thermal expansion for the Ca₂Ru_{0.98}Fe_{0.02}O₄,¹⁹ we chose not to apply substrate heat during the deposition process. A 25-nm-thick Co film was deposited directly on the *ab* plane of a single-crystal Ca₂Ru_{0.98}Fe_{0.02}O₄ substrate at room temperature with a deposition rate of 0.05 nm/s. The base pressure in the vacuum sputtering chamber was 10⁻⁷ Torr, while the working Ar pressure was 3 mTorr. No magnetic field was applied during the deposition process. X-ray diffraction showed that the Co film layers were polycrystalline. Measurements of both zero-field-cooled (ZFC) and field-cooled (FC) magnetizations $M(T,H)$ were performed using a Quantum Design Magnetic Property Measurement System (MPMS).

The FC process was performed by applying an external field within the film plane at 300 K and then cooling the samples down to the desired low temperatures.

III. RESULTS AND DISCUSSION

Figure 1(a) shows the magnetic susceptibility $\chi(T)$ for single-crystal $\text{Ca}_2\text{Ru}_{0.98}\text{Fe}_{0.02}\text{O}_4$ measured under $H = 70$ kOe for both ZFC and FC processes. The $\chi(T)$ curves exhibit an AFM phase transition at $T_N = 120$ K, which is similar to that observed for $\text{Ca}_2\text{Ru}_{1-x}\text{Fe}_x\text{O}_4$ with $x = 0.08$ or 0.12 .¹⁹ The isothermal magnetization data for a few representative temperatures for a single-crystal $\text{Ca}_2\text{Ru}_{0.98}\text{Fe}_{0.02}\text{O}_4$ substrate are shown in Figs. 1(b) and 1(c). The magnetic hysteresis loops exhibit linear behavior for $T < 60$ K, indicating AFM order, but also saturation typical of weak FM order, due to the onset of canted AFM order at 100 K.²²

Figure 2 shows typical FC hysteresis loops for a $\text{Co}/\text{Ca}_2\text{Ru}_{0.98}\text{Fe}_{0.02}\text{O}_4$ sample for different cooling fields. For each measurement, the sample was warmed up to 300 K and then cooled down to 5 K in magnetic fields of 0, 30, and 70 kOe, respectively. The left panel of Fig. 2 displays the magnetic hysteresis loops for a $\text{Co}/\text{Ca}_2\text{Ru}_{0.98}\text{Fe}_{0.02}\text{O}_4$ sample. Since the magnetization of the single-crystal $\text{Ca}_2\text{Ru}_{0.98}\text{Fe}_{0.02}\text{O}_4$ substrate is linear at 10 K [Fig. 1(b)], the FM hysteresis behavior seen in Fig. 2 must arise from the Co film deposited on the substrate. It is remarkable that the FC loops exhibit large horizontal and vertical shifts, while the ZFC loop lies symmetric about the origin. In order to adequately define the exchange bias field (H_E) and the vertical magnetization shift (M_E) from the tilted loops, we subtract the linear background from the original data in the left panel. This exercise produces square hysteresis loops shown in the right panel of Fig. 2, and yields the relevant parameters H_E , H_C , and M_E , as defined in Fig. 2(f).

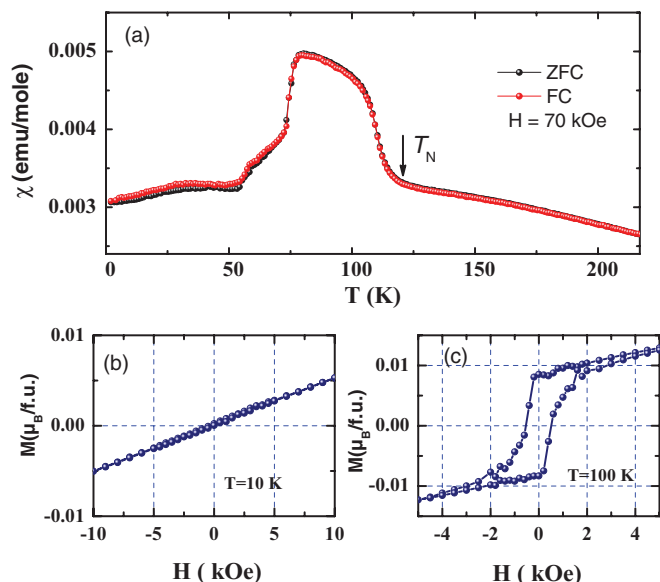


FIG. 1. (Color online) (a) $M(T)$ curves for single-crystal $\text{Ca}_2\text{Ru}_{0.98}\text{Fe}_{0.02}\text{O}_4$ measured under 70 kOe after ZFC and FC procedures. ZFC hysteresis loops for single-crystal $\text{Ca}_2\text{Ru}_{0.98}\text{Fe}_{0.02}\text{O}_4$ at $T = 10$ K are shown in (b), and for $T = 100$ K in (c).

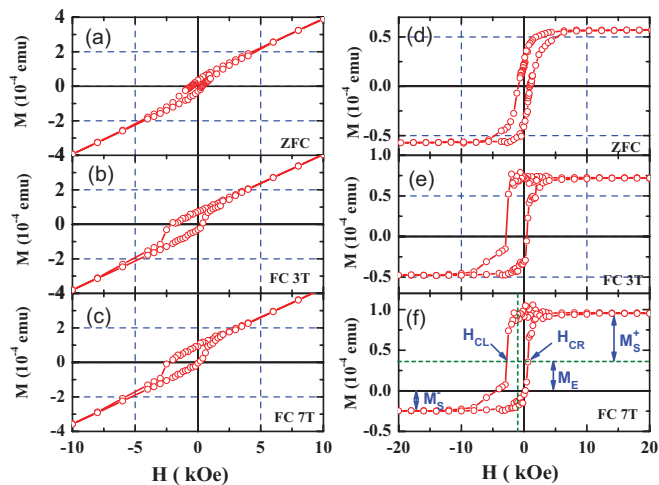


FIG. 2. (Color online) Representative hysteresis loops for $\text{Co}(25\text{nm})/\text{Ca}_2\text{Ru}_{0.98}\text{Fe}_{0.02}\text{O}_4$ measured at 10 K after field cooling at various fields: (a) and (d) 0 kOe, (b) and (e) 30 kOe, and (c) and (f) 70 kOe. The left panel shows raw data. The right panel shows the hysteresis loops after subtracting the linear AFM contribution of the single-crystal $\text{Ca}_2\text{Ru}_{0.98}\text{Fe}_{0.02}\text{O}_4$ substrate. The green dotted lines in (f) denote the new center of gravity of the FC loop.

The parameters, H_E , H_C , and M_E , which are obtained from the loops in the right panels of Fig. 2, are illustrated in Fig. 3(f). M_E is defined as the shift of the center of gravity of the hysteresis loop along the magnetization axis, and it is a measure of the average value of the saturation magnetizations at the positive and negative measuring fields (M_s^+ and M_s^- , respectively); i.e., $M_E = (M_s^+ + M_s^-)/2$. The exchange bias field can be deduced from the expression $H_E = |H_{CL} + H_{CR}|/2$, and the coercivity is $H_C = (H_{CR} - H_{CL})/2$, where H_{CL} and H_{CR} are defined in Fig. 2(f).

We use positive and negative cooling fields to determine the FC hysteresis loops, namely $+70$ and -70 kOe, as shown in Fig. 3. Two measurement processes are used to obtain a closed hysteresis loop after FC: (1) $(+H_{\text{max}}) \rightarrow 0 \rightarrow (-H_{\text{max}}) \rightarrow 0 \rightarrow (+H_{\text{max}})$ for the positive cooling field; (2) $(-H_{\text{max}}) \rightarrow 0 \rightarrow (+H_{\text{max}}) \rightarrow 0 \rightarrow (-H_{\text{max}})$ for the negative cooling field.

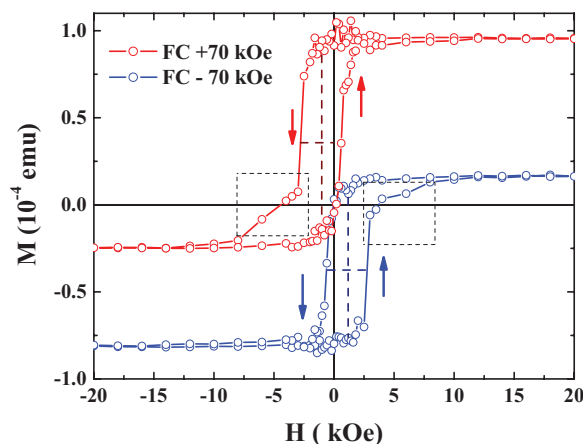


FIG. 3. (Color online) Hysteresis loops measured at 10 K for $\text{Co}/\text{Ca}_2\text{Ru}_{0.98}\text{Fe}_{0.02}\text{O}_4$ sample after ZFC (a) and FC in fields of $+70$ and -70 kOe (b).

The maximum measuring field H_{\max} is 20 kOe. It is clear that the direction of the horizontal loop shift is opposite to the cooling-field direction (Fig. 3). Furthermore, the saturated magnetization is much larger in the positive-field side when the sample is cooled in a positive field; similarly, the magnitude of the saturated magnetization is much larger in the negative-field side when the sample is cooled in a negative field. These results clearly illustrate that the *directions of the horizontal shift in the field and the vertical shift in the magnetization are both determined by the cooling-field direction*.²³ Indeed, an asymmetry between the two branches of the hysteresis loop for descending and ascending magnetic fields is generally characteristic of EB systems.^{3,24–26} However, the asymmetry displayed in Fig. 3 is unusual in that the descending branch, which is defined as the branch from $(+H_{\max}) \rightarrow 0 \rightarrow (-H_{\max})$ for positive cooling field and $(-H_{\max}) \rightarrow 0 \rightarrow (+H_{\max})$ for negative cooling field, is more extended compared to the ascending branch (see the dashed squares in Fig. 3). This asymmetry is intimately related to irreversible changes of the AFM domain structure during the magnetization reversal.³

The most striking effect we have observed is the large VMS, which constitutes up to 60% of the total magnetization for the cooling field of 70 kOe [Fig. 2(f)]. The large VMS indicates the presence of a large number of AFM pinned spins which are anchored in the antiferromagnet; the AFM pinned spins therefore contribute to the overall magnetization, leading to VMS. It is noted that large VMS is observed in other nonheterostructures, such as polycrystalline ceramics^{11,13,14} and nanoparticles,¹² in which the VMS is driven by different mechanisms, such as an incomplete reversal of the FM spins,^{11,13} or frozen, uncompensated spins in the spin-glass-like phase at the FM/spin-glass-like interface.^{12,14} In contrast, the VMS in conventional FM/AFM thin-film interfaces is associated with *uncompensated*, pinned AFM spins.⁸ In the case of $\text{Co}/\text{Ca}_2\text{Ru}_{0.98}\text{Fe}_{0.02}\text{O}_4$, the single-crystal $\text{Ca}_2\text{Ru}_{0.98}\text{Fe}_{0.02}\text{O}_4$ substrate is a *compensated*, G-type AFM in which there are no uncompensated AFM spins. A new model is therefore needed to explain the observed results.

To gain more insight into the mechanism of the giant VMS in $\text{Co}/\text{Ca}_2\text{Ru}_{0.98}\text{Fe}_{0.02}\text{O}_4$, we examine the effects of the cooling-field strength on the EB properties. As shown in Fig. 4, M_E increases markedly with increasing cooling field. On the other hand, H_C first increases with the increase of the cooling field and then saturates, whereas H_E is independent of the cooling-field strength. The observed behavior in the $\text{Co}/\text{Ca}_2\text{Ru}_{0.98}\text{Fe}_{0.02}\text{O}_4$ system represents a departure from the behavior of conventional FM/AFM thin-film interfaces (where *both* M_E and H_E are usually independent of the cooling-field strength, and M_E is almost zero) in hysteresis loop measurements.^{2,3}

We offer a scenario to explain the observed behavior. The $\text{Co}/\text{Ca}_2\text{Ru}_{0.98}\text{Fe}_{0.02}\text{O}_4$ system is expected to have an interfacial spin configuration, as illustrated in Fig. 5. The Ru(Fe) spins lie in the ab plane, and the canted spin structure results in net FM moments. The net FM moments of the first monolayer for the $\text{Ca}_2\text{Ru}_{0.98}\text{Fe}_{0.02}\text{O}_4$ align parallel to the Co spins due to the exchange interaction at the interface when the system is field cooled; and the next monolayer of the AFM then aligns antiparallel to the first layer, and so forth. Given the proximity effect and the two-dimensional nature

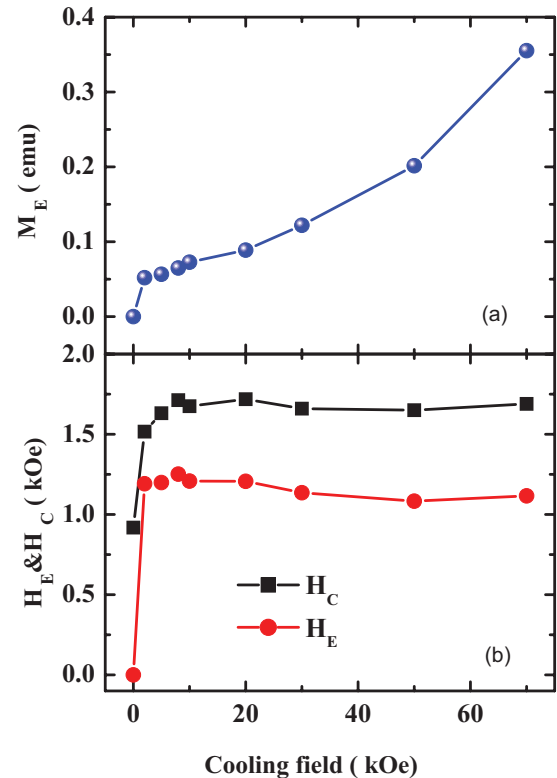


FIG. 4. (Color online) Cooling-field dependence of the vertical shift M_E (a), exchange bias field H_E and coercivity H_C (b) for $\text{Co}/\text{Ca}_2\text{Ru}_{0.98}\text{Fe}_{0.02}\text{O}_4$ system.

of $\text{Ca}_2\text{Ru}_{0.98}\text{Fe}_{0.02}\text{O}_4$, the interfacial coupling occurs only between the first monolayer of $\text{Ca}_2\text{Ru}_{0.98}\text{Fe}_{0.02}\text{O}_4$ and the Co spins. When the direction of the field is reversed, there is a tendency for the Co spins to reverse their direction as well; however, because of the strong coupling between the Co spin and the Ru (Fe) spins, it takes more energy, thus a stronger external field, to overcome the microscopic torque and rotate the Co spins. As a result, the hysteresis loop shifts toward the negative field and H_E becomes nonzero. At the same time,

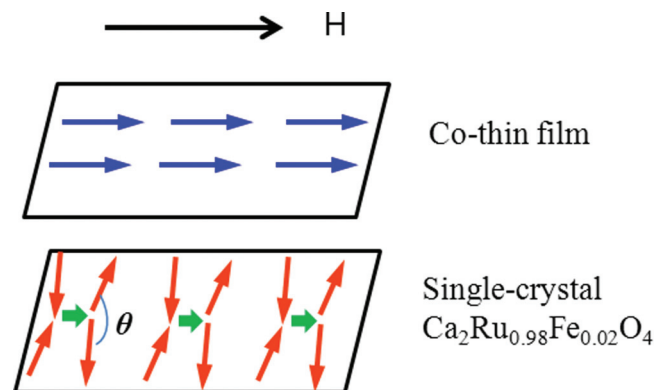


FIG. 5. (Color online) Spin configuration at the $\text{Co}/\text{Ca}_2\text{Ru}_{0.98}\text{Fe}_{0.02}\text{O}_4$ interface. The upper (blue) and lower (red) arrows represent the FM (Co) and AFM (Ru or Fe) spins. The short and thick (green) arrows represent the net FM moments of the canted Ru (Fe) spins. θ is the canting angle between the Ru (Fe) spins.

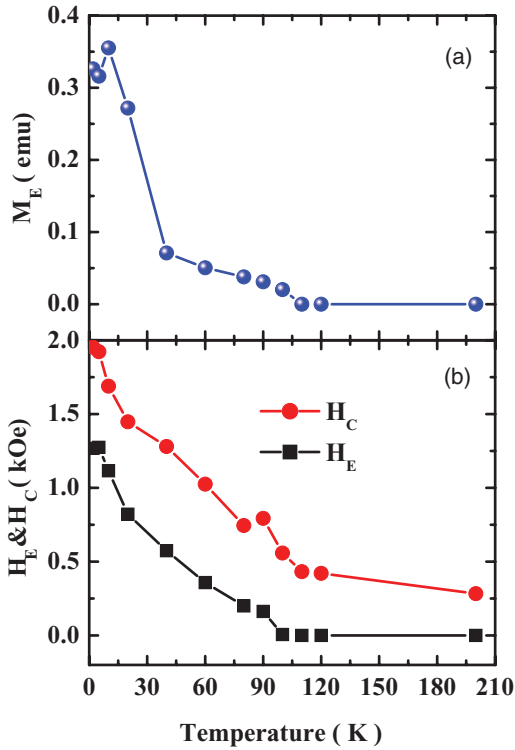


FIG. 6. (Color online) Temperature dependence of the vertical shift M_E (a), exchange bias field H_E and coercivity H_C (b), for the Co/Ca₂Ru_{0.98}Fe_{0.02}O₄ system.

the net FM moments of Ru (Fe) cannot readily be rotated with a reversed magnetic field, leading to an upward shift of the hysteresis loop. The cooling-field strength can affect the canting angle θ between the Ru (Fe) spins; specifically, the net FM moments of Ru (Fe) increase with increasing cooling field. Thus, the VMS increases due to the contribution of the net FM moments, which explains the observed M_E .

We confirm the above scenario by investigating the temperature dependence of EB properties or the training effect, which describes the decrease of the exchange bias field when cycling the system through several consecutive hysteresis loops. In these measurements, in order to overcome the influence of the training effect on the EB, the sample was first cooled down from 250 K to the measuring temperature under a magnetic field of 70 kOe. Once the measuring temperature was reached, the magnetic hysteresis loop was measured between -20 and 20 kOe. This process was repeated for every measuring temperature. As presented in Fig. 6, H_E and H_C decrease with increasing temperature and H_E appears to vanish at 110 K (blocking temperature), which is in the vicinity of T_N of single-crystal Ca₂Ru_{0.98}Fe_{0.02}O₄. H_E and H_C hardly change above T_N as the temperature is increased further. The temperature evolution of H_E and H_C is typical of most EB systems. The vertical shift M_E exhibits a trend similar to that for H_E and H_C , despite a brief drop in M_E at $T < 10$ K, which might be related to changes of the canting angle. Since the canting angle of Ru (Fe) spins is expected to increase with increasing temperature for Ca₂Ru_{0.98}Fe_{0.02}O₄, the net FM moment of Ru (Fe) decreases. Therefore, M_E , which arises

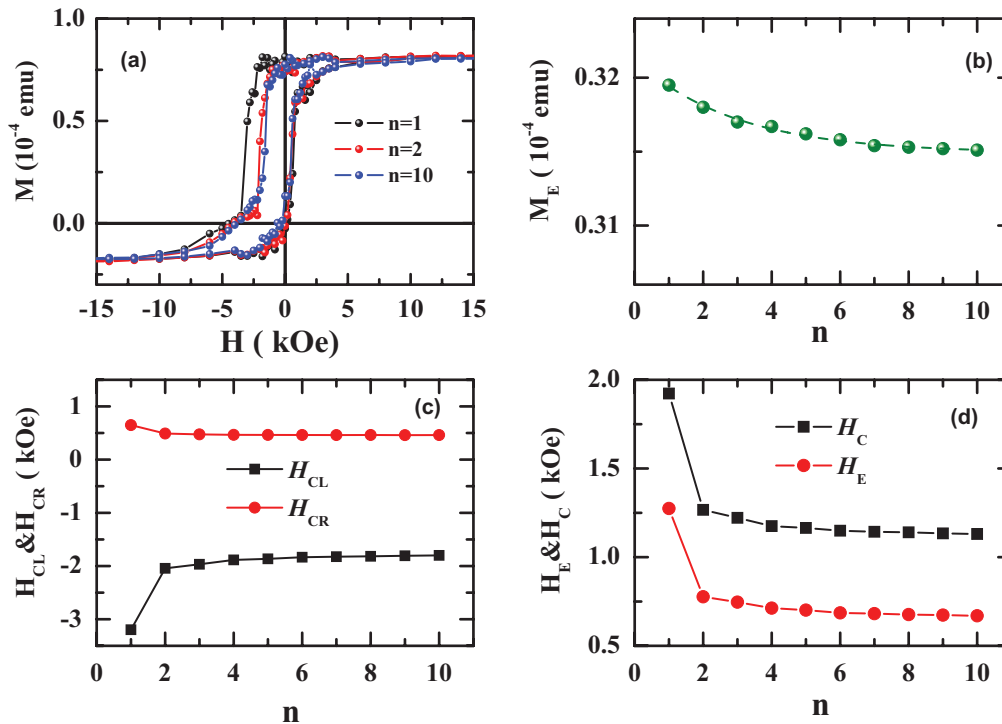


FIG. 7. (Color online) Training effect of the Co/Ca₂Ru_{0.98}Fe_{0.02}O₄ system. (a) Hysteresis loops measured at temperature $T = 5$ K after field cooling under 70 kOe from 250 down to 5 K. The black, red, and blue solid circles represent the first, second, and tenth hysteresis loops, respectively. (b) M_E as a function of the field cycle number n . The dashed line is a simple power-law fit. (c) Coercive fields H_{CL} and H_{CR} , and (d) H_E and H_C as functions of the field cycle number n . The straight lines connecting the squares and circles in (b) and (d) are guides to the eye.

from the net FM moment as discussed above, decreases with increasing temperature, as shown in Fig. 6(a).

The EB decreases when the sample undergoes a number of consecutive measurements of magnetic hysteresis loops, n . Figure 7(a) shows the first, second, and tenth hysteresis loops of the sample after field cooling down to 5 K under 70 kOe. The first loop exhibits $H_E = 1275$ Oe, but this value decreases to 649 Oe when $n = 10$. In comparison, M_E weakly decreases, as shown in Fig. 7(b). This is reasonable since the canting angle between Ru (Fe) spins should remain unchanged during these consecutive measurements of the hysteresis loops. The absolute values of H_{CL} and H_{CR} are also plotted as a function of n in Fig. 7(c). It is seen that the training effect is more prominent in the descending curve than in the ascending curve of the hysteresis, i.e., H_{CL} decreases drastically while H_{CR} changes only slightly. The loop shrinks from both sides with the cycle of the applied field [such a training effect is defined as Type I (Ref. 27)]. The decay of H_E and H_C as functions of n are shown in Fig. 7(d); it is obvious that approximately 80% of the training dynamics takes place between the first and second loop.

IV. CONCLUSIONS

In summary, we have deposited a Co film on a compensated, G-type AFM $\text{Ca}_2\text{Ru}_{0.98}\text{Fe}_{0.02}\text{O}_4$ single crystal. A central finding of this work is the giant vertical magnetization shift observed in the $\text{Co}/\text{Ca}_2\text{Ru}_{0.98}\text{Fe}_{0.02}\text{O}_4$ heterostructure that is seldom seen in other heterostructures. All experimental evidence indicates that the VMS primarily arises from the net FM moments resulting from the canted spin configuration of single-crystal $\text{Ca}_2\text{Ru}_{0.98}\text{Fe}_{0.02}\text{O}_4$. It is conceivable that the giant vertical magnetization shift could be observed in other heterostructures consisting of G-type antiferromagnets.

ACKNOWLEDGMENTS

This work was supported by the US NSF through Grants No. DMR0856234 and No. EPS-0814194, and NSFC (Grants No. 11274221 and No. 50932003). L.E.D. is supported by US DoE Grant No. DE-FG02-97ER45653. S.J.Y. acknowledges the Research Innovation Fund of the Shanghai Education Committee Grant No. 12YZ018.

*Corresponding author: shujuanyuan@shu.edu.cn

¹W. H. Meiklejohn and C. P. Bean, *Phys. Rev.* **105**, 904 (1957).

²J. Nogués and I. K. Schuller, *J. Magn. Magn. Mater.* **192**, 203 (1999).

³F. Radu and H. Zabel, in *Magnetic Heterostructures*, edited by H. Zabel and S. Bader (Springer, Berlin, Heidelberg, 2008), Vol. 227, pp. 97–184.

⁴M. Kiwi, *J. Magn. Magn. Mater.* **234**, 584 (2001).

⁵J. Nogués, C. Leighton, and I. K. Schuller, *Phys. Rev. B* **61**, 1315 (2000).

⁶U. Nowak, K. D. Usadel, J. Keller, P. Miltényi, B. Beschoten, and G. Güntherodt, *Phys. Rev. B* **66**, 014430 (2002).

⁷J. Keller, P. Miltényi, B. Beschoten, G. Güntherodt, U. Nowak, and K. D. Usadel, *Phys. Rev. B* **66**, 014431 (2002).

⁸H. Ohldag, A. Scholl, F. Nolting, E. Arenholz, S. Maat, A. T. Young, M. Carey, and J. Stöhr, *Phys. Rev. Lett.* **91**, 017203 (2003).

⁹H. Ohldag, H. Shi, E. Arenholz, J. Stöhr, and D. Lederman, *Phys. Rev. Lett.* **96**, 027203 (2006).

¹⁰A. Mumtaz, K. Maaz, B. Janjua, S. K. Hasanain, and M. F. Bertino, *J. Magn. Magn. Mater.* **313**, 266 (2007).

¹¹Y.-K. Tang, Y. Sun, and Z.-H. Cheng, *Phys. Rev. B* **73**, 174419 (2006).

¹²Z. M. Tian, S. L. Yuan, S. Y. Yin, L. Liu, J. H. He, H. N. Duan, P. Li, and C. H. Wang, *Appl. Phys. Lett.* **93**, 222505 (2008).

¹³S. Yuan, K. Xu, Z. Li, L. Yu, B. Kang, and S. Cao, *J. Appl. Phys.* **105**, 093910 (2009).

¹⁴Z. M. Tian, S. L. Yuan, X. F. Zheng, L. C. Jia, S. X. Huo, H. N. Duan, and L. Liu, *Appl. Phys. Lett.* **96**, 142516 (2010).

¹⁵J. de la Venta, M. Erekhinsky, S. Wang, K. G. West, R. Morales, and I. K. Schuller, *Phys. Rev. B* **85**, 134447 (2012).

¹⁶L. Q. Yan, W. Ren, J. Shen, Z. H. Sun, and F. W. Wang, *J. Appl. Phys.* **105**, 07A719 (2009).

¹⁷D. Mauri, H. C. Siegmann, P. S. Bagus, and E. Kay, *J. Appl. Phys.* **62**, 3047 (1987).

¹⁸A. P. Malozemoff, *Phys. Rev. B* **35**, 3679 (1987).

¹⁹T. F. Qi, O. B. Korneta, S. Parkin, J. Hu, and G. Cao, *Phys. Rev. B* **85**, 165143 (2012).

²⁰T. F. Qi, O. B. Korneta, S. Parkin, L. E. De Long, P. Schlottmann, and G. Cao, *Phys. Rev. Lett.* **105**, 177203 (2010).

²¹T. F. Qi, M. Ge, O. B. Korneta, S. Parkin, L. E. De Long, and G. Cao, *J. Solid State Chem.* **184**, 893 (2011).

²²Y. B. Bazaliy, L. T. Tsymbal, G. N. Kakazei, A. I. Izotov, and P. E. Wigen, *Phys. Rev. B* **69**, 104429 (2004).

²³P.-H. Huang, H.-H. Huang, and C.-H. Lai, *Appl. Phys. Lett.* **90**, 062509 (2007).

²⁴V. I. Nikitenko, V. S. Gornakov, A. J. Shapiro, R. D. Shull, K. Liu, S. M. Zhou, and C. L. Chien, *Phys. Rev. Lett.* **84**, 765 (2000).

²⁵M. R. Fitzsimmons, P. Yashar, C. Leighton, I. K. Schuller, J. Nogués, C. F. Majkrzak, and J. A. Dura, *Phys. Rev. Lett.* **84**, 3986 (2000).

²⁶M. R. Fitzsimmons, C. Leighton, A. Hoffmann, P. C. Yashar, J. Nogués, K. Liu, C. F. Majkrzak, J. A. Dura, H. Fritzsche, and I. K. Schuller, *Phys. Rev. B* **64**, 104415 (2001).

²⁷K. Zhang, T. Zhao, and H. Fujiwara, *J. Appl. Phys.* **91**, 6902 (2002).